

Tracing the evolution of the symmetry energy of hot nuclear fragments from the compound nucleus towards multifragmentation

G. A. Souliotis¹, A. S. Botvina², D. V. Shetty¹, A. L. Keksis¹, M. Jandel^{1,*}, M. Veselsky^{1,†} and S. J. Yennello¹

¹ *Cyclotron Institute, Texas A&M University, College Station, TX 77843 and*

² *Institute for Nuclear Research, Russian Academy of Sciences, RU-117312 Moscow, Russia*
(Dated: May 25, 2019)

The evolution of the symmetry energy coefficient of the binding energy of hot fragments with increasing excitation is explored in multifragmentation processes following heavy-ion collisions below the Fermi energy. In this work, high-resolution mass spectrometric data on isotopic distributions of projectile-like fragments from collisions of 25 MeV/nucleon ⁸⁶Kr and ⁶⁴Ni beams on heavy neutron-rich targets are systematically compared to calculations involving the Statistical Multifragmentation Model. The study reveals a gradual decrease of the symmetry energy coefficient from 25 MeV at the compound nucleus regime ($E^*/A \leq 2$ MeV) towards 15 MeV in the bulk multifragmentation regime ($E^*/A \geq 4$ MeV). The ensuing isotopic distributions of the hot fragments are found to be very wide and extend towards the neutron drip-line. These findings may have important implications to the composition and evolution of hot astrophysical environments, such as core-collapse supernova.

PACS numbers: 25.70.-z, 25.70.Hi, 25.70.Lm

Nuclear multifragmentation is one of the most interesting phenomena in nuclear physics as it holds great promise for understanding nuclear matter properties at the extreme conditions of high excitation energy and large isospin (N/Z) asymmetry [1, 2, 3, 4, 5]. The latter, in particular, plays a profound role in the dynamics and evolution of various astrophysical environments [6, 7, 8, 9]. It is well known that nuclear systems with relatively low excitation energy ($E^*/A \leq 2$ MeV) form the traditional compound nucleus, which deexcites via light-particle evaporation and/or fission. At higher excitation energy, the hot nuclear system first expands to subsaturation density and, subsequently, splits into an ensemble of hot nuclear fragments (primary fragments). This extremely complicated process, namely the multifragmentation, occurs on a timescale of 100 fm/c (3.3×10^{-22} sec) during which the system can sample a large number of configurations. For this reason, statistical calculations (e.g., [10, 11]) have been very successful in describing this process.

Recently, a remarkable similarity has been pointed out between the thermodynamic conditions reached in nuclear multifragmentation and the collapse/explosion of massive stars [12, 13, 14], offering the possibility of applying well-established nuclear models to describe matter distribution in supernova [12]. In addition, statistical calculations suggest that in multifragmentation [12, 15] and in hot astrophysical environments (e.g. supernova) [12, 16], the ensemble of primary fragments includes neutron-rich nuclei towards or beyond the neutron drip-line.

The primary fragments are hot and, initially, in close proximity to neighboring fragments or nucleonic gas. These conditions render their properties, e.g. binding energy, different from those of cold isolated nuclei. In particular, recent studies [17, 18, 19, 20] give evidence for

a significant decrease of the symmetry energy of hot primary fragments. It is well known that for a system with N neutrons and Z protons, the symmetry energy [i.e., the excess energy relative to the symmetric configuration ($N=Z$)] can be expressed as $E_{\text{sym}} = C_{\text{sym}}(N - Z)^2/A$, with C_{sym} the symmetry energy coefficient and A the mass number [21]. In the aforementioned studies, the symmetry energy of hot fragments from multifragmentation at high excitation energy ($E^*/A = 4-6$ MeV) is found to be reduced to $C_{\text{sym}} \sim 15$ MeV or lower, as compared to the conventional value of $C_{\text{sym}} \sim 25$ MeV for cold nuclei. In the same vein, our recent work [22] indicated decreased symmetry energy of hot heavy fragments in the region $E^*/A=2-3$ MeV. The observed reduction of the symmetry energy implies that more neutron-rich nuclei are favored in the distribution of fragments after the partitioning of the initial hot and expanded nuclear system. Such unusual neutron-rich nuclei should also be quite abundant in supernova matter [12] and may affect the dynamics of the explosion and the subsequent nucleosynthesis. Herein, fragments with $A > 40$ are referred to as heavy residues, those with $A < 40$ as heavy IMF (intermediate mass fragments), whereas both groups are collectively called heavy fragments.

The present Letter is intended to provide evidence for a continuous evolution of the symmetry energy coefficient from the compound nucleus regime ($E^*/A \leq 2$ MeV) towards multifragmentation ($E^*/A \geq 4$ MeV) by a systematic comparison of the isotopic distributions of heavy fragments with calculations based on the Statistical Multifragmentation Model (SMM). Moreover, the N/Z distributions of hot nuclei from the multifragmentation of neutron-rich systems are found to be very wide involving exotic nuclei towards the neutron drip-line.

The experimental data were obtained at the Cyclotron Institute of Texas A&M University. Two mag-

netic separators were used: MARS (Momentum Achromat Recoil Separator) for the ^{86}Kr (25 MeV/nucleon) + ^{64}Ni , ^{124}Sn , ^{208}Pb reactions and the Superconducting Solenoid Line (BigSol) for the ^{64}Ni (25 MeV/nucleon) + ^{64}Ni reaction. A detailed description of the measurements is presented in [22, 23, 24]. However, an outline is given in the following. For the MARS measurements, a 25 MeV/nucleon ^{86}Kr beam (~ 1 pnA) from the K500 superconducting cyclotron interacted with ^{64}Ni and ^{124}Sn targets at 4.0° relative to the optical axis of MARS. Fragments were accepted in the angular range 2.7° – 5.4° . At the focal plane, the fragments were collected in a ΔE – E Si detector telescope. Time of flight was measured between two PPACs (parallel plate avalanche counters) at the MARS dispersive image and at the focal plane, respectively. The horizontal position from the first PPAC and the field of the MARS first dipole magnet determined the magnetic rigidity, $B\rho$. With the procedures of [24], the atomic number Z , the ionic charge q , the mass number A and the velocity were obtained with high resolution (0.5, 0.4, 0.6 units and 0.3%, respectively). After summation over ionic charge states, fragment cross sections with respect to Z , A and velocity were obtained in the angular range 2.7° – 5.4° and $B\rho$ range 1.3–2.0 T m. The measurements of the ^{86}Kr (25 MeV/nucleon) + ^{208}Pb were performed in the angular range 1.0° – 2.7° (with the beam hitting the target at 0° and with an on-axis blocker collecting the unreacted beam – as in [24]) and $B\rho$ range 1.2–1.7 T m. Finally, the ^{64}Ni (25 MeV/nucleon) + ^{64}Ni measurements were performed with the Superconducting Solenoid Line (BigSol) in the angular range 1.5° – 3.0° and $B\rho$ range 1.1–1.6 T m, as in the latter MARS measurement. The measured yield distributions (summed over velocity) were used to extract the average Z/A values as a function of fragment mass. To obtain total fragment cross sections, the measured yield data were corrected for the limited angular acceptance and magnetic rigidity range of the measurements (as in [24]) with the aid of the simulations described below.

The calculations are based on a two-stage Monte Carlo approach. The dynamical stage of the collision was described by the deep-inelastic transfer (DIT) code of Tassan-Got [25] simulating stochastic nucleon exchange in peripheral and semiperipheral collisions. This model has been successful in describing the isospin, excitation energy and kinematical properties of excited quasiprojectiles in a number of studies at Fermi energies [24, 26, 27, 28]. The deexcitation of the quasiprojectiles was performed with the latest version of the Statistical Multifragmentation Model (SMM) [10, 14, 29], referred to as “SMM05” and briefly summarized below. The model assumes statistical equilibrium at a low-density freeze-out stage. It includes all breakup channels ranging from the compound nucleus to vaporization (channels with only light particles $A < 4$), allowing a unified description of nuclear disintegration with increasing ex-

citation. In the microcanonical treatment, the statistical weight of a decay channel is calculated as exponential of the entropy of the system in this channel. Light fragments with $A < 4$ are considered as stable particles (nuclear gas) with only translational degrees of freedom. Fragments with $A > 4$ are treated as heated nuclear liquid drops with free energies parameterized as a sum of volume, surface, Coulomb and symmetry energy terms [14] with parameters adopted from the Bethe-Weizsacker mass formula. In the freeze-out configuration, it is assumed that these hot fragments are isolated and at normal density. These hot fragments propagate independently in their mutual Coulomb field, while undergoing deexcitation via evaporation, fission or Fermi breakup [10]. The model generates a Markov chain of partitions (by employing the Metropolis algorithm) representative of the whole partition ensemble [29]. The Coulomb interaction energy is directly calculated for each spatial configuration of fragments in the freeze-out volume. Finally, the effect of the Coulomb field of the target is included. The symmetry energy evolution is taken into account in the mass calculation for the primary and the secondary fragments during the sequential evaporation process. Below a threshold of $E^*/A = 1$ MeV, a smooth transition to standard experimental masses is assumed as in [14]. Standard parameters of the SMM code are employed in the calculations. In particular, a multiplicity dependent parametrization of the free volume (determining the contribution of the fragment translational motion to the partition probability [10]) is used, whereas, the freeze-out volume (defining the Coulomb energy of the fragment partition) is taken to be 6 times the nuclear volume at normal density (as suggested by the asymptotic velocities of the observed heavy fragments).

Fig. 1 shows the average proton fraction $\langle Z/A \rangle$ of the fragments with respect to mass for the reactions presented in order of increasing system N/Z . The experimental data are shown by solid symbols and span the whole range of masses from evaporation residues down to heavy IMF. Vertical arrows indicate an approximate separation between heavy residues from evaporation and from the onset of multifragmentation. The thin solid line (marked “SL”) gives the line of β stability and the thin dotted line (marked “EAL”) represents the evaporation attractor line [30]. The evaporation residue regime is populated by neutron deficient fragments, except for the heaviest fragments from $^{86}\text{Kr} + ^{64}\text{Ni}$ and $^{86}\text{Kr} + ^{124}\text{Sn}$ corresponding to very peripheral products [23]. Fragments on the left side of the arrow (produced, according to our calculations, above the multifragmentation threshold of $E^*/A \sim 2$ MeV) show progressively smaller values of Z/A and cross the line of β stability (Fig. 1).

The results of the DIT/SMM05 calculations are presented by thick lines. The dotted lines correspond to calculations with constant values of the symmetry energy of $C_{\text{sym}} = 25, 20, 15$ MeV from the upper to the

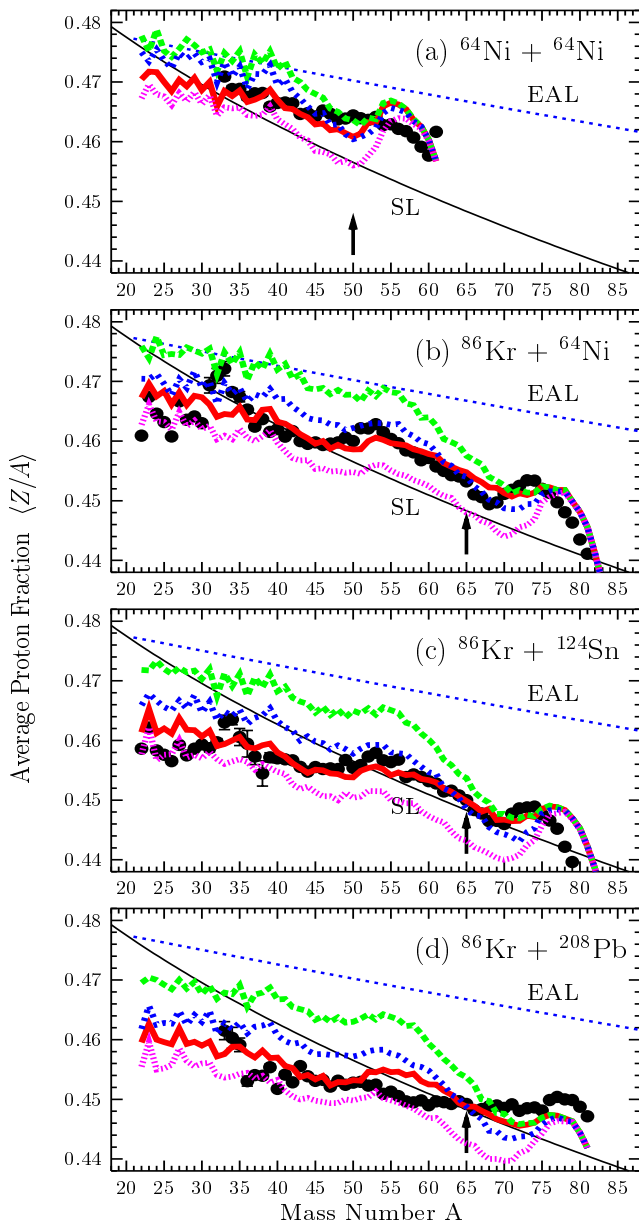


FIG. 1: (Color Online) Average Z/A vs. A . (a) ^{64}Ni (25 MeV/nucleon) + ^{64}Ni (BigSol data). (b),(c),(d) ^{86}Kr (25 MeV/nucleon) + ^{64}Ni , ^{124}Sn , ^{208}Pb , respectively (MARS data). Solid points: data. Thin solid line (SL): line of stability. Thin dotted line (EAL): evaporation attractor line. Thick lines: DIT/SMM05 calculations. Dotted lines, top to bottom: with $C_{\text{sym}} = 25, 20, 15$ MeV, respectively. Thick solid line: with the form of $C_{\text{sym}}(E^*/A)$ given by the thick line in Fig. 2. Arrows: multifragmentation vs compound nucleus regime (see text).

lower lines. We observe that the standard calculation with $C_{\text{sym}}=25$ MeV produces fragments that are, on average, more neutron deficient than the observed fragments. With $C_{\text{sym}}=20$ MeV, the agreement with the data seems to improve, except for the lowest masses, whereas with $C_{\text{sym}}=15$ MeV, only the latter group of masses is de-

scribed. We point out that the measured heavy fragment data at 25 MeV/nucleon span a continuous range of excitation energies up to $E^*/A = 4$ MeV (and slightly above). With the intuitive assumption of a continuous behavior of the symmetry energy from low towards high excitation, we tested various forms of the dependence of C_{sym} on excitation energy E^*/A (see below). We found that the dependence presented by the thick solid line in Fig. 2 [assigning $C_{\text{sym}}=15$ MeV to the small fraction of events with $E^*/A > 4$ MeV], is able to provide a remarkable agreement of the calculations with the heavy fragment data from multifragmentation-like processes (to the left of the arrow), as shown by the solid lines in Fig. 1.

The thin solid lines in Fig. 2 indicate two of the various forms of $C_{\text{sym}}(E^*/A)$ dependence that we tested in the SMM05 calculations. The results of $\langle Z/A \rangle$ for Kr+Sn are shown in Fig. 3 by thin solid lines (the lower one corresponding to the left thin line of Fig. 2 and the upper one to the right thin line of Fig. 2). In Fig. 3, we notice that the thin lines embrace the thick line obtained with the final form of $C_{\text{sym}}(E^*/A)$ dependence (thick line in Fig. 2), as mentioned above. Similar results are obtained for the other reactions studied in this work. We may consider the thin solid lines in Fig. 2 as indicative of the region of uncertainty in the symmetry energy evolution as obtained from the comparisons of the present implementation of the SMM model with our heavy fragment data.

Summarizing, as illustrated in Fig. 2, the symmetry energy coefficient appears to decrease linearly from 25 MeV at $E^*/A \sim 2$ MeV and below (compound nucleus regime – left arrow in Fig. 2) to 15 MeV at $E^*/A \sim 4$ MeV (bulk multifragmentation regime – right arrow in Fig. 2). This phenomenological evolution of the symmetry energy coefficient of hot heavy fragments is the main result of the present Letter.

For further comparison, in Fig. 2 we include the values of the symmetry energy coefficient obtained in our recent work on the isoscaling analysis of heavy fragments from ^{86}Kr (circle, square) and ^{64}Ni (triangle) reactions [22]. We notice that, in spite of the different approach of symmetry energy determination, an overall agreement in the trend is observed – with a systematically lower position of the points, however, possibly associated with temperature determination (see [22]). Furthermore, the present results point to substantially lower symmetry energy in the bulk multifragmentation regime, $E^*/A \sim 4$ MeV and above, in overall qualitative agreement with the reduced values of the symmetry energy for multifragmentation reported by the recent studies [17, 18, 19, 20], as stated earlier. We note that the behavior of the symmetry energy coefficient with excitation observed in this work and the aforementioned previous studies may originate from in-medium modifications of the properties of the hot primary fragments in their dense surroundings [31]. Microscopic calculations are necessary to shed light

on this very interesting and challenging issue [32].

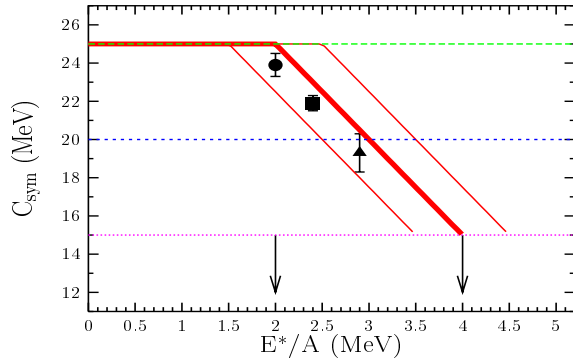


FIG. 2: (Color online) Thick solid line: final form of $C_{\text{sym}}(E^*/A)$ dependence employed in the SMM05 calculations. Thin solid lines: other forms of $C_{\text{sym}}(E^*/A)$ dependence used in the calculations shown in Fig. 3 (see text). Thin horizontal lines (from top to bottom): $C_{\text{sym}} = 25, 20, 15$ MeV, respectively, as used in the calculations of Fig. 1. Solid points: values of C_{sym} from ^{86}Kr (circle, square) and ^{64}Ni (triangle) induced reactions from the isoscaling analysis of [22].

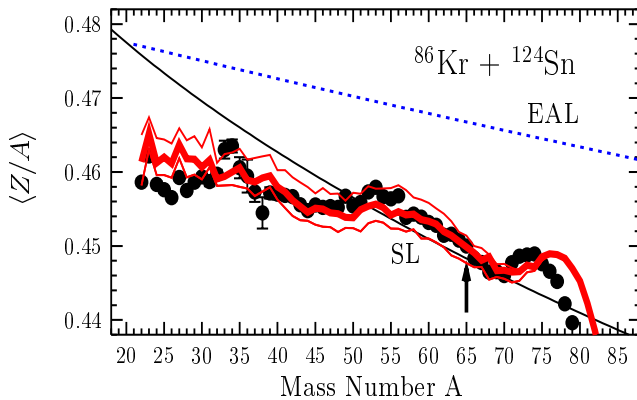


FIG. 3: (Color Online) Average Z/A vs A for ^{86}Kr (25 MeV/nucleon) + ^{124}Sn . Solid points (data), lines SL, EAL and arrow as in Fig. 1. Solid lines: DIT/SMM05 calculations corresponding to the forms of $C_{\text{sym}}(E^*/A)$ dependence presented by the corresponding lines in Fig. 2 (see text).

Apart from the average Z/A properties, the present calculations are able to describe the various characteristics of the observed fragments including the widths of the isotopic mass distributions, the velocity distributions and the production cross sections. A full report on these results is currently underway. For completeness, we present in Fig. 4, a comparison of the experimental mass distributions with the DIT/SMM05 calculations for several reactions: $^{86}\text{Kr}+^{64}\text{Ni}$ and $^{86}\text{Kr}+^{208}\text{Pb}$. The final form of $C_{\text{sym}}(E^*/A)$ dependence (thick line in Fig. 2) was used in these calculations. For Kr+Ni, the data (which have the highest counting statistics) are

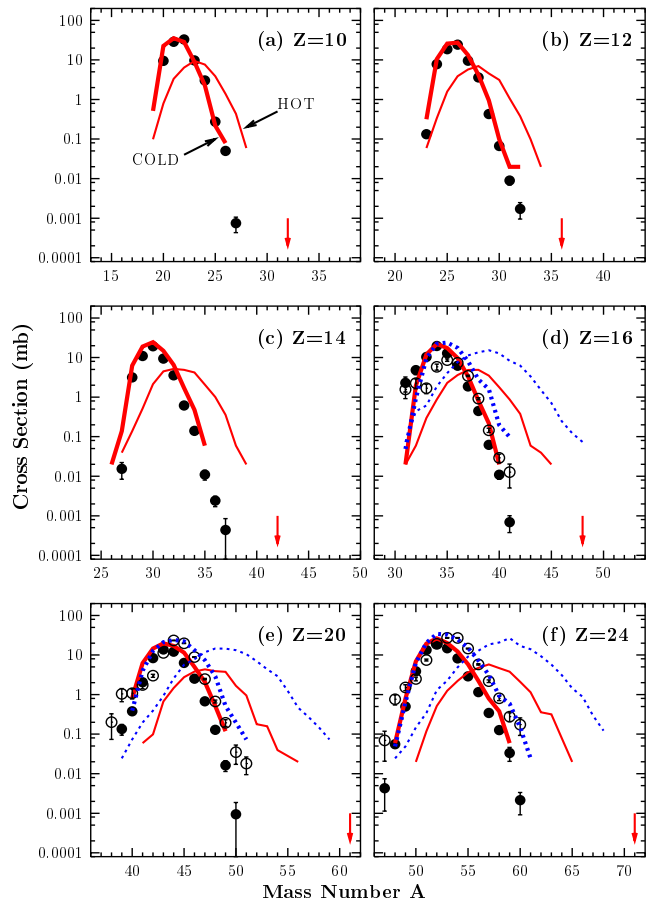


FIG. 4: (Color online) Comparison of experimental mass distributions of several elements with DIT/SMM05 calculations (see text). Solid points: data from ^{86}Kr (25 MeV/nucleon)+ ^{64}Ni . Open points: data from ^{86}Kr (25 MeV/nucleon)+ ^{208}Pb . Full lines: DIT/SMM05 calculations for $^{86}\text{Kr}+^{64}\text{Ni}$; thick: final (cold) fragments, thin: primary (hot) fragments. Dotted lines: DIT/SMM05 calculations for $^{86}\text{Kr}+^{208}\text{Pb}$; thick: final (cold) fragments, thin: primary (hot) fragments (see text). Arrows: neutron-drip line [33].

shown by the full circles and the calculations by the thick solid lines (the thin solid lines giving the hot primary fragment distributions for these elements). Similarly, for Kr+Pb, the data are given by open circles and the calculations by thick dotted lines (again, the thin dotted lines describing hot fragments). We find an overall satisfactory agreement of the calculations with the mass distribution data. Interestingly, the Kr+Pb data extend to more neutron-rich products than those of Kr+Ni (demonstrating the significant role of the target N/Z at this energy regime [23, 28]), a trend accurately described by the calculation. Finally, we note that the distributions of the hot primary fragments are wide and lie to the neutron-rich side of the nuclear chart. Particularly, for the Kr+Pb reaction (the most neutron-rich system studied), they are very wide and extend towards the neutron drip-line [33] (arrows in Fig. 4). The calculations indicate that the dis-

tributions of these hot exotic nuclei are sensitive to their masses which, in turn, are sensitive to the evolution of the symmetry energy with excitation.

We believe that comparisons of high-resolution heavy fragment data with precise model calculations as in the present work can provide valuable information on the distributions and the properties of hot and very neutron-rich nuclei towards the neutron drip-line. A natural extension of these endeavors in the future is the study of reactions with very neutron-rich rare beams on heavy neutron-rich targets in RIB facilities, such as the Rare Isotope Accelerator (RIA) facility (e.g. [34]). Knowledge on the properties of exotic nuclei produced in hot and dense environments are essential for astrophysical calculations, such as the composition and dynamics of core-collapse supernova and the course of the relevant nucleosynthesis processes (e.g., the r process).

In conclusion, a gradual evolution of the symmetry energy coefficient of the nuclear binding energy with respect to excitation is observed in the multifragmentation following heavy-ion collisions below the Fermi energy. In the present work, experimental data on isotopic distributions of projectile-like fragments from peripheral and semiperipheral collisions of 25 MeV/nucleon ^{86}Kr and ^{64}Ni beams on heavy targets are compared to calculations with the Statistical Multifragmentation Model. The study indicates a gradual decrease of the symmetry energy coefficient from 25 MeV at $E^*/A \sim 2$ MeV and below (compound nucleus regime) towards 15 MeV at $E^*/A \sim 4$ MeV and above (multifragmentation regime). The isotopic distributions of the hot fragments following the multifragmentation stage are very wide, and extend to exotic neutron-rich nuclei. These findings are of importance in calculations of the isotopic composition in hot and dense astrophysical environments, such as those encountered in supernova.

We are thankful to L. Tassan-Got for his DIT code. We gratefully acknowledge the support of the operations staff of the Cyclotron Institute during the measurements. Financial support for this work was provided, in part, by the U.S. Department of Energy under Grant No. DE-FG03-93ER40773 and by the Robert A. Welch Foundation under Grant No. A-1266. A.S.B was supported in part through grant RFFR 05-02-04013 (Russia) and M.V. in part through grant VEGA-2/5098/25 (Slovak Scientific Grant Agency).

[†] Institute of Physics of the Slovak Academy of Sciences, Bratislava, Slovakia.

- [1] V. Baran, M. Colonna, V. Greco, and M. DiToro, *Phys. Rep.* **410**, 335 (2005).
- [2] P. Chomaz, M. Colonna, and J. Randrup, *Phys. Rep.* **389**, 263 (2004).
- [3] P. Danielewicz, R. Lacey, and W. G. Lynch, *Science* **298**, 1592 (2002).
- [4] J. Richert and P. Wagner, *Phys. Rep.* **350**, 1 (2001).
- [5] L. G. Moretto, R. Ghetti, L. Phair, K. Tso, and G. J. Wozniak, *Phys. Rep.* **287**, 249 (1997).
- [6] A. W. Steiner, M. Prakash, J. M. Lattimer, and P. J. Ellis, *Phys. Rep.* **411**, 325 (2005).
- [7] J. M. Lattimer and M. Prakash, *Science* **304**, 536 (2004).
- [8] S. Woosley and T. Janka, *Nature Physics* **1**, 147 (2005).
- [9] B. A. Li and W. U. Schröder, eds., *Isospin Physics in Heavy Ion Collisions at Intermediate Energies* (Nova Science, New York, 2001).
- [10] J. P. Bondorf, A. S. Botvina, A. S. Iljinov, I. N. Mishustin, and K. Sneppen, *Phys. Rep.* **257**, 133 (1995).
- [11] D. H. E. Gross, *Rep. Prog. Phys.* **53**, 605 (1990).
- [12] A. S. Botvina and I. N. Mishustin, *Phys. Lett. B* **584**, 233 (2004).
- [13] A. S. Botvina and I. N. Mishustin, *Phys. Rev. C* **72**, 048801 (2005).
- [14] N. Buyukcizmeci, R. Ogul, and A. S. Botvina, *Eur. Phys. J. A* **25**, 57 (2005).
- [15] S. Pratt, W. Bauer, C. Morling, and P. Underhill, *Phys. Rev. C* **63**, 034608 (2000).
- [16] C. Ishizuka, A. Ohnishi, and K. Sumiyoshi, *Nucl. Phys. A* **723**, 517 (2003).
- [17] J. Iglío et al., *Phys. Rev. C* accepted, nucl-ex/0512011 (2006).
- [18] D. V. Shetty et al., *Phys. Rev. C* **71**, 024602 (2005).
- [19] A. LeFèvre et al., *Phys. Rev. Lett.* **94**, 162701 (2005).
- [20] D. Henzlova et al., nucl-ex/0507003 (2005).
- [21] K. Heyde, *Basic Ideas and Concepts in Nuclear Physics* (Institute of Physics Publishing, Bristol and Philadelphia, 1994).
- [22] G. A. Souliotis et al., *Phys. Rev. C* **73**, 024606 (2006).
- [23] G. A. Souliotis et al., *Phys. Rev. Lett.* **91**, 022701 (2003).
- [24] G. A. Souliotis et al., *Phys. Lett. B* **543**, 163 (2002).
- [25] L. Tassan-Got and C. Stefan, *Nucl. Phys. A* **524**, 121 (1991).
- [26] M. Veselsky et al., *Phys. Rev. C* **62**, 064613 (2000).
- [27] M. Veselsky et al., *Nucl. Phys. A* **724**, 431 (2003).
- [28] G. A. Souliotis, M. Veselsky, D. V. Shetty, and S. Y. Yennello, *Phys. Lett. B* **588**, 35 (2004).
- [29] A. S. Botvina and I. N. Mishustin, *Phys. Rev. C* **63**, 061601 (2001).
- [30] R. Charity, *Phys. Rev. C* **58**, 1073 (1998).
- [31] A. S. Botvina and I. N. Mishustin, nucl-th/0510081 (2005).
- [32] M. Beyer, S. Strauss, P. Schuck, and S. A. Sofianos, *Eur. Phys. J. A* **22**, 261 (2004).
- [33] P. Moller, J. R. Nix, and K. L. Kratz, *At. Data Nucl. Data Tables* **66**, 131 (1997).
- [34] J. A. Nolen, *Nucl. Phys. A* **746**, 9 (2004).

* C-INC, Los Alamos National Laboratory, Los Alamos, NM 87545.